RESEARCH ARTICLE

Botany

Estimating carbon assimilation rates from fossil leaves and application to the mid-Miocene Clarkia forest

Melanie R. Cham[1] | Alexander J. Lowe[2,3] | Dana L. Royer[1] |
Sophia M. Ronan[4] | William C. Rember[5] | Caroline A. E. Strömberg[2,3]

[1]Department of Earth and Environmental Sciences, Wesleyan University, Middletown, Connecticut 06459, USA

[2]Department of Biology, University of Washington, Seattle, Washington 98195, USA

[3]Burke Museum of Natural History and Culture, University of Washington, Seattle, Washington 98195, USA

[4]Department of Biology, University of North Carolina Greensboro, Greensboro, North Carolina 27412, USA

[5]Independent researcher, Fernwood, Idaho 83830, USA

Correspondence
Melanie R. Cham, Department of Earth and Environmental Sciences, Wesleyan University, Middletown, Connecticut 06459, USA.
Email: mcham@wesleyan.edu

Abstract

Premise: The rate of carbon assimilation in leaves (A) is a key trait central to a plant's economic strategy that has downstream impacts on the regional and global cycling of carbon and other nutrients. Most previous paleoecological studies estimate A from nearest living relatives or leaf vein density.

Methods: We present a method for reconstructing A using gas-exchange modeling that requires both measured (stomatal size and density, leaf $\delta^{13}C$) and inferred (e.g., atmospheric CO_2 concentration) inputs. We apply this method to ten extant taxa and nine fossil taxa representing common angiosperms of the exquisitely preserved mid-Miocene (~15.9 Ma) flora at Clarkia in northern Idaho, USA.

Results: Application to extant taxa produces estimates of A that are near measured values on the same leaves ($R^2 = 0.89$ across all taxa). Median reconstructed A for fossil taxa range from 9.5–21.7 μmol m^{-2} s^{-1} with 95% confidence intervals ~+51%/−38% indicating that most species are statistically indistinguishable. Sensitivity tests show that our method is most reliable when CO_2 is well-constrained, but when that is impractical, taxa within single sampling horizons (with a presumed fixed CO_2 concentration) can be organized by A into a relative rank order with tighter confidence intervals (~+16%/−14%).

Conclusions: Following this relative approach at Clarkia, we reconstruct high A for taxa whose modern relatives are characterized by rapid growth and/or riparian habitats (*Castanea* and *Platanus*) and corroborate previous interpretations on the ecology of taxa whose modern relatives are less known (*Quercus simulata*).

KEYWORDS
carbon assimilation rates, fossil leaves, leaf stomata, leaf-gas exchange model, Miocene, paleobotany, paleoecology, photosynthesis

Photosynthetic carbon assimilation is the process by which plants take in CO_2 to generate chemical energy in the form of glucose. Its rate (A) is a core trait of the leaf-economic spectrum, which is a suite of intercorrelated traits related to how fast (or slow) a plant acquires and turns over nutrient resources (Reich, 2014). This spectrum is strongly linked to growth strategy, including the turnover of plant parts and the subsequent cycling of carbon, nitrogen, and phosphorus (Cornwell et al., 2008).

Reconstructing A from fossil plants is critical for understanding the ecology of past plant communities, the evolutionary ecology of plant lineages (e.g., Boyce et al., 2009), and their downstream impacts on global biogeochemical cycles (e.g., McElwain et al., 2024). Assimilation rates of fossil taxa are often inferred from rates measured in nearest living relatives (NLRs) (e.g., Reichgelt and D'Andrea, 2019). By definition, this approach assumes that A is evolutionarily conservative, which is partly at odds with the observation that the leaf-economic spectrum in plants today generally reflects evolutionary convergence (Ackerly and Reich, 1999; Donovan et al., 2011); additionally, environmental variables such as temperature, light, and water availability may affect A, resulting in variation even within a taxon (e.g., Bassow and Bazzaz, 1997). Another method for estimating A is based on the direct fossil measurement of leaf vein density, which often scales strongly with A (Brodribb et al., 2010; Blonder et al., 2011) although sometimes only weakly, particularly within angiosperms (e.g., Sack et al., 2013; $r = 0.34$).

Here we introduce a method for estimating A in fossil plants based on leaf gas-exchange principles that is complementary to existing techniques but that, unlike the NLR method, does not require an assumption of conserved physiology within species and, compared to the vein density method, is statistically more robust. We first describe the model and test it on extant taxa where A is measured directly. Second, we apply the method to a suite of fossil angiosperm taxa at the well-known mid-Miocene site at Clarkia, Idaho, and compare our results to those based on NLRs and vein density. Third, we perform a sensitivity analysis to identify the inputs whose uncertainties most affect estimated A and explore how generalizable the analysis at Clarkia is to other fossil localities. Lastly, for individual sites with poorly constrained atmospheric CO_2 concentrations (but an assumed fixed value), we highlight the value of comparing relative (rank order) differences in A across taxa.

MODEL DESCRIPTION

Our method is based on a well-vetted model for leaf carbon assimilation, A (µmol m^{-2} s^{-1}) (Farquhar and Sharkey, 1982), where $g_{c(tot)}$ is the total operational conductance to CO_2 diffusion from the atmosphere to the site of photosynthesis (mol m^{-2} s^{-1}) and c_a and c_i represent the concentration of CO_2 in the air and intercellular spaces, respectively (µmol mol^{-1} or ppm):

$$A = g_{c(tot)} \cdot (c_a - c_i) \tag{1}$$

We then expand Equation (1) to be expressed in a manner more easily calculated from fossils:

$$A = g_{c(tot)} \cdot c_a (1 - c_i/c_a) \tag{2}$$

For fossil applications, c_a is estimated from paleo-CO_2 proxies (e.g., Hönisch et al., 2023); c_i/c_a is estimated from measurements of leaf $\delta^{13}C$ and reconstructions of air $\delta^{13}C$ (e.g., Tipple et al., 2010) following Farquhar and Sharkey (1982), where a and b are, respectively, the carbon isotopic fractionations associated with diffusion of CO_2 in air (4.4‰; Farquhar and Sharkey, 1982) and with RuBP carboxylase (30‰; Roeske and O'Leary, 1984):

$$\frac{c_i}{c_a} = \frac{\frac{\delta^{13}C_{air} - \delta^{13}C_{leaf}}{1 + \delta^{13}C_{leaf}/1000} - a}{b - a} \tag{3}$$

and $g_{c(tot)}$ is estimated largely from measurements of stomatal size and density following Franks et al. (2014), where g_{cb} is the leaf boundary layer conductance to CO_2, $g_{c(max)}$ is the maximum stomatal conductance to CO_2, z scales $g_{c(max)}$ to operational stomatal conductance to CO_2, and g_m is mesophyll conductance:

$$g_{c(tot)} = \left(\frac{1}{g_{cb}} + \frac{1}{\zeta g_{c(max)}} + \frac{1}{g_m} \right)^{-1} \tag{4}$$

$g_{c(max)}$ can be further broken down to:

$$g_{c(max)} = \frac{\frac{d}{v} \cdot D \cdot a_{max}}{l + \frac{\pi}{2}\sqrt{\frac{a_{max}}{\pi}}} \tag{5}$$

where D is stomatal density (m^{-2}), l is stomatal pore depth (m), a_{max} is the maximum area of a single stomatal pore (m^2), and d/v is the ratio of diffusivity of CO_2 in air to the molar volume of air (mol m^{-1} s^{-1}), respectively.

MODEL IMPLEMENTATION

Our approach largely parallels a leaf gas-exchange model developed by Franks et al. (2014), which also uses stomatal anatomy and carbon isotopic composition measured from leaf fossils as inputs. The key difference is that our model solves for A, while Franks et al. (2014) rearrange Equation (1) to solve for c_a, forming the basis for a thoroughly tested paleo-CO_2 proxy (Royer et al., 2019; Hönisch et al., 2023). Because c_a is an input for our model, we use values derived from methods other than the Franks model to avoid circularity.

According to Equations 4–5, the fossil measurements that contribute to $g_{c(tot)}$ are stomatal density (D); stomatal pore length, which is then scaled to a_{max} (if not observable, pore length can be scaled from guard cell length; see Franks et al., 2014 for details); and the width of a single guard cell, which is then generally scaled to stomatal depth (l) (Franks et al., 2014). Inputs for $g_{c(tot)}$ that are inferred (not measured) include boundary layer conductance (g_{cb}), which is assumed fixed at 2 mol m^{-2} s^{-1} (Franks et al., 2014); mesophyll conductance (g_m), which is scaled from A based on measurements in extant plants (Franks et al., 2014); and the scaling between operational and maximum stomatal conductance to CO_2 ($g_{c(op)}/g_{c(max)}$ or ζ), which is also based on measurements in extant plants (Franks et al., 2014; Royer et al., 2019; Murray et al., 2019, 2020). For these inferred inputs, we follow the recommendations of Franks et al. (2014): a value of 0.2 for ζ, a stomatal depth equal to the width of a single guard cell, and (for C$_3$ angiosperms) circular stomatal pores when the pores are fully open. For the Franks CO_2 model, plausible ranges in ζ and A have the largest impact on the uncertainties in estimated CO_2 (Maxbauer et al., 2014; Kowalczyk et al., 2018; Milligan et al., 2019). In contrast to the Franks CO_2 model, in our model we are solving for A and c_a is an input; our model is thus strongly influenced by input choices for ζ and c_a.

We implemented our model in the R environment (version 2023.09.1 + 494; R Core Team, 2023); see Appendix S1 for the code and Appendix S2: Table S1 for an example input file.

Because we use A to model g_m, A appears on both sides of Equation (2); thus, we solve Equation (2) and the estimate of g_m iteratively until the estimate of A converges. Similar to the Franks CO_2 model, we propagate uncertainties in all inputs in a Monte Carlo framework (we recommend 10,000 resamples) to generate a probability density function, from which the median A and 95% confidence interval can be extracted.

It is common to estimate median A and its 95% confidence interval at the species level based on measurements of multiple fossil leaves (e.g., Zhang et al., 2024). One approach to do this is to first compute the means and standard errors of each measured input across the population of leaves and then run the model once. But this can lead to spurious results because most inputs in the model behave nonlinearly with A and because multiple combinations of inputs are consistent with a single value of A (in other words, each leaf is a unique biosensor). Instead, we strongly recommend running the model for each leaf first and then aggregating the leaf-level results to species level.

We explore two ways to aggregate leaf-level probability density functions: inverse-variance weighting and "means". We implemented both approaches in R (Appendix S3); both use the raw resamples as their input (see Appendix S4: Table S2 for an example) and analyze the leaf-level probability distributions of these resamples. Inverse-variance weighting prioritizes the intervals of A across leaves with the most overlap. The "means" approach calculates the mean of each resample, i.e., for a species with five leaves and 10,000 resamples, for example, the mean of the first resample of the five leaves is computed, then the second resample, and so on, until a string of 10,000 means is generated. The species-level probability is then based on these 10,000 means. Probabilistically, it behaves similarly to a standard error of the mean.

When the probability distributions of the individual leaves strongly overlap, we find that both methods yield comparable results. In cases where leaf-level distributions do not overlap, we find that inverse-variance weighting produces very narrow uncertainty windows that we consider overly optimistic. Thus, all our taxon-level confidence intervals are based on the "means" approach. We do caution here that strongly non-overlapping distributions at the leaf level may warrant a red flag that some model assumptions have been violated, for example that the leaves come from different canopy positions or multiple species or were deposited across enough time for the atmospheric CO_2 concentration to have changed.

MATERIALS AND METHODS

Living plants

We tested our model in ten extant species (two angiosperms, six gymnosperms, and two ferns) using published stomatal, isotopic, and physiological data from: (1) field-grown trees from Franks et al. (2014) (*Quercus robur* L.

(Fagaceae), *Cycas revoluta* Thunb. (Cycadaceae), *Sequoia sempervirens* Endl. (Taxodiaceae), *Ginkgo biloba* L. (Ginkgoaceae)), Maxbauer et al. (2014) (*Metasequoia glyptostroboides* Hu and W.C.Cheng (Taxodiaceae)), and Kowalczyk et al. (2018) (*Ginkgo biloba* and *Sassafras albidum* (Nutt.) Nees. (Lauraceae)); and (2) chamber-grown juveniles grown at 484 and 1274 ppm CO_2 from Franks et al. (2014) (*Wollemia nobilis* W.G. Jones, K.D. Hill and J.M. Allen (Araucariaceae)) and at 500 and 1000 ppm from Milligan et al. (2019) (*Cedrus deodara* (Roxb. ex D.Don) G.Don (Pinaceae), *Osmundastrum cinnamomeum* (L.) C.Presl (Osmundaceae), and *Stenochlaena palustris* (Burm.f.) Bedd. (Blechnaceae)). The assimilation rates in these studies were measured using a LI-COR infrared gas analyzer (Li-Cor Inc., Lincoln, Nebraska, USA). In all cases, we compared our modeled assimilation rates to rates measured directly on the same leaves.

Fossil site

We applied our model to a fossil assemblage to evaluate its ability to reconstruct plausible values of A. We focused on nine woody angiosperm species from site P37 (Emerald Creek) of the Clarkia fossil lake Lagerstätte in Idaho, USA; this locality is ideal because of its exquisite preservation of compression fossils that is related to anoxic bottom waters at the time of deposition (see Smiley and Rember, 1985b for background information about the site). The age of P37 is constrained to ~15.9 Ma (earliest middle Miocene) based on chemical correlations of tuffs to radiometrically dated extrabasinal tuffs (Ladderud et al., 2015; Geraghty, 2017), representing the height of the Miocene Climatic Optimum (MCO; 17–14 Ma). The MCO was the most recent period of sustained global warming, with an estimated CO_2 of ~450–550 ppm (Steinthorsdottir et al., 2021b; Liang et al., 2022), offering an analog to 21st century anthropogenic climate change (Steinthorsdottir et al., 2021a). Based on local contemporaneous paleosols, the climate at Clarkia was warm and humid, unlike northern Idaho today (Smiley and Rember, 1985a; Rember, 1991; Hobbs and Parrish, 2016). Consistent with this inferred climate, many taxa found at Clarkia are common today in the southeast USA (Rember, 1991). Based on the warmer, wetter climate and higher CO_2 levels reconstructed for Clarkia, we predict that A will be higher than its modern relatives.

We collected leaves from a single 40 cm layer, 115 cm below ash P37-8 (Ladderud et al., 2015; Geraghty, 2017) and identified them to the finest possible taxonomic level. The sampled taxa are *Acer chaneyi* Knowlton (Aceraceae, $n = 5$ leaves), *Betula vera* Brown (Betulaceae; $n = 6$), *Betula fairii* Knowlton (Betulaceae; $n = 5$), *Castanea spokanesis* (Knowlton) R.W. Chaney and D.I. Axelrod (Fagaceae; $n = 8$), Fabaceae ($n = 6$), Lauraceae ($n = 6$), *Platanus dissecta* Lesquereux (Platanaceae, $n = 6$), *Quercus payettensis* Knowlton (Fagaceae; $n = 7$), and *Quercus simulata* Knowlton (Fagaceae; $n = 11$; identical to "*Lithocarpus simulata*" of Rember, 1991).

We separated leaves from their rock matrix by applying 5–10 mL of 48% hydrofluoric acid to the center of the surface of the fossil. After about 5 minutes, we neutralized the fossil and rock matrix with deionized water and then gently scraped off the intact leaf (Rember, 1991; see Appendix S5 for additional details); the lifted leaves retain their (ad-/abaxial) epidermal cellular detail (Figure 1). All leaves are archived individually in 5% hydrochloric acid in plastic containers in the laboratory cold storage at the Burke Museum of Natural History and Culture (Seattle, Washington, USA). For microscopy and imaging, the leaves were rinsed and mounted onto slides with deionized water.

Constraining CO_2 at mid-Miocene site

Atmospheric CO_2 concentrations are required for reconstructing A with our model (see Equation 2). We estimate a mean CO_2 value from the multi-proxy compilation of Hönisch et al. (2023) within 250 kyrs of our site (mean = 538 ppm; n = 25 proxy estimates), excluding estimates based on leaf gas-exchange modeling (n = 3) to remove potential for circularity. Because the uncertainties both within and across the CO_2 estimates are lognormal, we assume in our code a lognormal distribution modeled from the mean (538 ppm) and 16th percentile (399 ppm). None of the estimates in this compilation can be correlated confidently to the exact age of our site, which poses a potential problem because CO_2 during the MCO may have varied ~200 ppm on 100 kyr timescales (Greenop et al., 2014). We thus take confidence that leaf-gas exchange estimates of CO_2 at our site (median = 491 ppm; 95% confidence = 466–521 ppm; Steinthorsdottir et al., 2021b) and a neighboring site 12–13 m below our site (P33 or Fossil Bowl

and Racetrack; median = 592 ppm, 95% confidence = 512–700 ppm; Steinthorsdottir et al., 2021b, Liang et al., 2022) are similar to and bracket our composite estimate. We emphasize that to avoid circularity when estimating A, we do not use any CO_2 values derived from leaf gas-exchange theory nor from Clarkia fossils.

Isotopic measurements

We subsampled each fossil leaf for $\delta^{13}C$ analysis. The subsamples were wrapped in tin capsules for analysis in either the IsoLab at the Department of Earth and Space Sciences of the University of Washington (UW; Seattle, Washington, USA) or the Light Stable Isotope Mass Spec Lab at the Department of Geological Sciences of the University of Florida (UF; Gainesville, Florida, USA; see Appendix S5 for details). We analyzed forty-five samples at UW and thirty-six samples in duplicate at UF with an average difference between duplicates of 0.48‰, a value within characteristic intraleaf bulk $\delta^{13}C$ variation (Royer and Hren, 2022).

Stomatal measurements

We used the remaining fossil leaf tissue for stomatal and vein density measurements. We found that epifluorescence was sufficient to view the epidermal features on the lifted leaves without fully clearing the cuticle, although additional cleaning of the leaves was sometimes required to completely remove obstructing sediment (procedure detailed in Appendix S5). Leaves were viewed under epifluorescence using either a Leica (Wetzlar, Germany) DMLB microscope with a 420–490 nm filter cube and a mounted Jenoptik (Jena, Germany) Gryphax
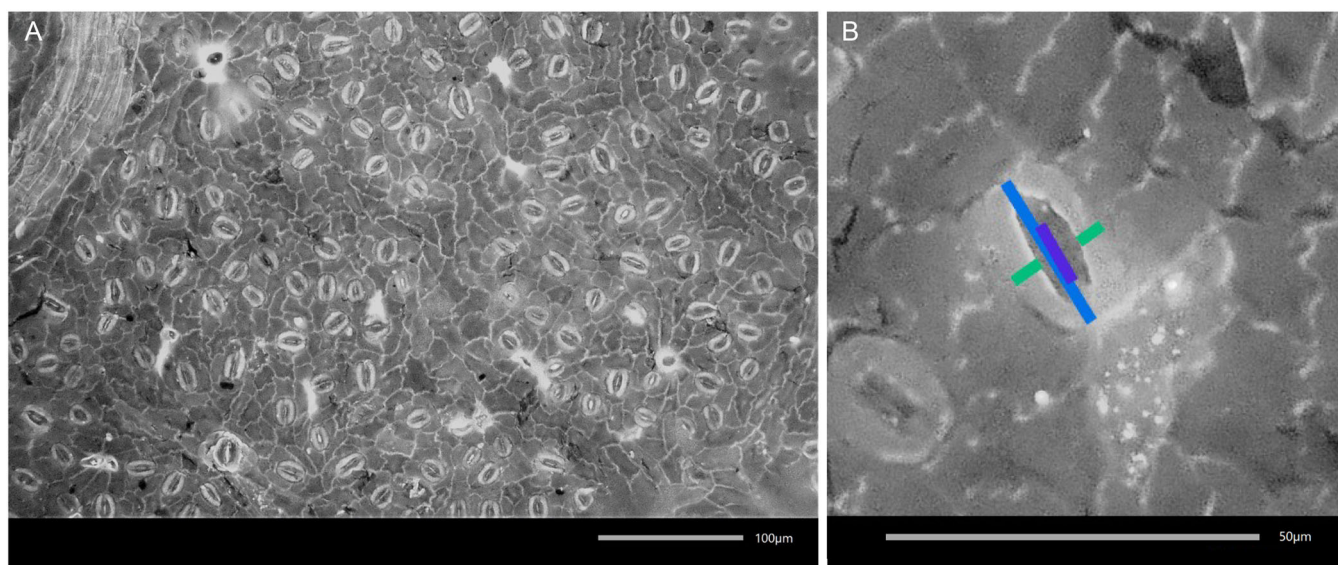

FIGURE 1 (A) Abaxial surface of *Castanea spokanesis* at 200× under epifluorescence; bar = 100 μm. (B) Pore length (purple), guard cell length (blue), and guard cell width (green) measurements on *C. spokanesis* at 400× under epifluorescence; bar = 50 μm.

digital microscope camera or a Nikon (Tokyo, Japan) LV100 microscope with neutral density filter 2 and a mounted Nikon Fi3 camera (Figure 1). For each leaf, we photographed seven representative z-stacked fields-of-view (FOVs) of the abaxial surface at 200× magnification for stomatal density and at 400× for stomatal pore length and single guard cell width, avoiding major veins and leaf margins (Jones and Rowe, 1999). For specimens whose pore length could not be measured reliably, we instead measured guard cell length and scaled to pore length using a scaling calibrated from other specimens of the same taxon whose pores and guard cell lengths could both be measured. We used Fiji (Schindelin et al., 2012) to measure the stomatal geometry traits on 10 stomata per leaf in at least two FOVs (Figure 1B). For stomatal density, we counted stomata in a demarcated 300 × 300 μm area. Stomata intersected at any part of the box were counted as 'in'. See Appendix S6 for a summary of all fossil measurements.

Vein density

To clear fossil tissue for vein density measurements, we isolated a 2–3 × 1–1.5 cm rectangle midway between the base and apex of each leaf, ideally between the margin and midvein. Fragments were rinsed with deionized water (DI), then placed into 3% hydrogen peroxide and a small amount of baking soda until cleared (typically 3–8 hours but ranging from less than an hour to several days). After clearing, we photographed the leaves at 60× where all veins were intact and visible but avoiding primary and secondary veins. Measurements were taken in a 2 mm² region on at least three FOVs. We used Fiji to measure the total length of veins (mm) per leaf area (mm²).

Nearest Living Relatives (NLRs)

We gathered area-based assimilation rates from the TRY plant database (https://www.try-db.org/TryWeb/Home.php) for 350 extant species in the same families or genera as our Clarkia taxa (Appendix S6: Table S5). We used the WorldFlora package in R (Kindt, 2020) to sort the NLR genera into families corresponding to our family level fossil taxon. Assimilation data on *Platanus* were not available in TRY and were taken instead from Milligan et al. (2022).

Sensitivity

We conducted a sensitivity analysis to assess which inputs have the most effect on estimated A. For atmospheric CO_2 we assume an uncertainty range equal to the minimum and maximum proxy estimates from the data set subsetted from Hönisch et al. (2023), which was 299–910 ppm. For all leaf-based inputs (c_i/c_a, $g_{c(tot)}$, stomatal density, stomatal pore length, single guard cell width, and leaf $\delta^{13}C$), the taxon ranges are equal to their leaf-level minima to maxima (x-axes in Figure 5B–G).

We assessed model sensitivity a second way by comparing the standard model run (Figure 6 "all") to modified runs where the uncertainty of only one input is included, and all other input uncertainties are set to zero. Lastly, we additionally assessed model sensitivity to atmospheric CO_2 by running the inverse: all inputs had their standard uncertainties *except* CO_2, whose uncertainty we set to zero; distributions in estimated A for these runs are shown as vertical bars adjacent to the violins in Figure 3.

RESULTS

Model testing in living plants

Estimates of A based on our model of leaf gas-exchange have 95% confidence bands at the species level that average +19%/ −17% of the median values. The median estimates are strongly and significantly correlated with A measured directly on the same leaves, irrespective of growth CO_2 concentration (Figure 2). Most estimates are statistically indistinguishable from their measured values: their 95% uncertainty bands overlap with the 1:1 dashed line in Figure 2. Furthermore, a standard major axis regression through the mean data has an r^2 value of 0.89 and its slope (0.81) is only marginally different from 1 (P = 0.04).

Application of model to fossil plants

Across our nine fossil taxa, the taxon-median A ranges from 9.5 to 21.7 μmol m⁻² s⁻¹ (open points in Figure 3), with a horizon median of 14.4 μmol m⁻² s⁻¹. These estimates are associated with considerable uncertainty. Within individual leaves, the propagated 95% confidence bands in A average +152%/−83% of the median estimates. Within a single taxon, the propagated 95% confidence bands average +51%/ −38% of the median estimates (black vertical lines within violins in Figure 3), considerably larger than in our modern test (+19%/−17%); importantly, the confidence bands across all taxa, except *Betula fairii* and *Castanea spokanesis*, overlap (Figure 3). Intraspecific leaf variability can be attributed to both model uncertainty and true variation in assimilation rate caused by differences in temperature, light, water availability, etc. (Ellsworth and Reich, 1993; Abrams, 1994; Šantrůček et al., 2014; Reichgelt and D'Andrea, 2019; Liu et al., 2023).

Comparison to other methods for constraining A

Assimilation rates estimated from NLRs correlate non-significantly with our model estimates both according to a standard major axis regression (Figure 4A; R² = 0.48, P = 0.09) and according to a Spearman's rank-order correlation (ρ = 0.36; P = 0.44).
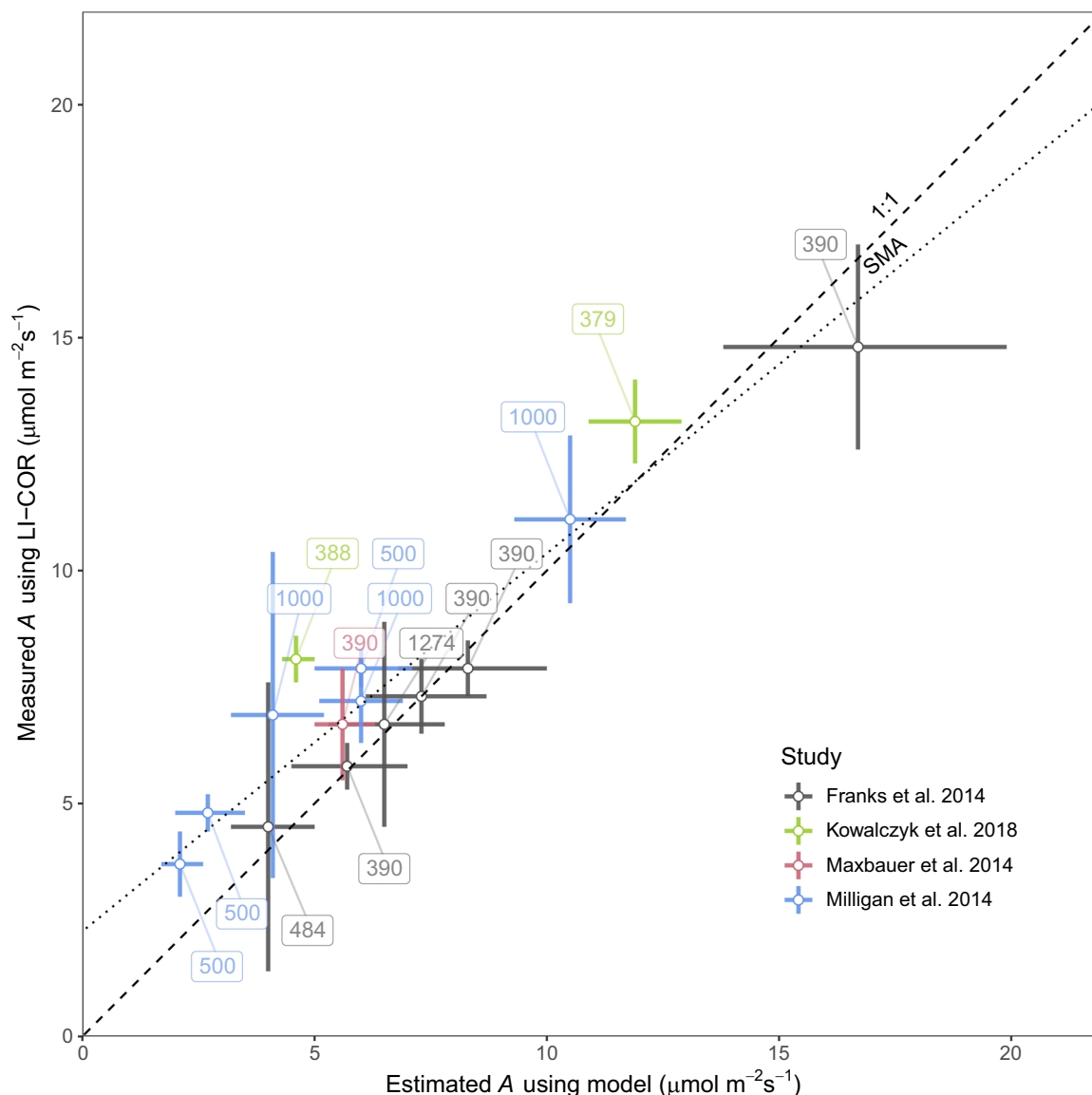
|

FIGURE 2 Estimated assimilation rate (A) using our model vs. measured A using a LI-COR based on four studies comprising ten species. Dashed line shows 1:1 correlation. Dotted line shows standard major axis regression: $y = 0.81x + 2.26$, $R^2 = 0.89$, $P < 0.001$. Labels inside boxes are the growth CO_2 concentration. Hollow dots are means. Bars are ±2 standard errors of the mean for measured A and 95% confidence bands for estimated A.

In contrast, vein densities measured on the same fossil specimens are uncorrelated with our modeled estimates according to a Spearman's rank-order test (Figure 4B; $\rho = 0$; $P = 1.00$). The two alternative methods (NLR and vein density) are also uncorrelated with one another (Figure 4C; $\rho = 0$; $P = 1.00$). Together, this suggests that vein density is not a good predictor for A at our site.

Sensitivity of A to variations in the input values

Our sensitivity analysis show that, of the three master variables (Figure 5A–C, panels with blue backgrounds; see Equation 2), CO_2 is the most sensitive. Even when c_i/c_a and $g_{c(tot)}$ are broken down into their constituent parts (stomatal density, pore length, guard cell width, leaf $d^{13}C$; Figure 5D–G, panels with yellow backgrounds), plausible ranges in CO_2 still have the most outsized impact on estimated A. This remains true even when a more constrained CO_2 range is assumed (16–84th percentile; shaded region in Figure 5A).

Although we derive our mean CO_2 estimate from the compilation of Hönisch et al. (2023), some individual studies suggest higher CO_2 (e.g., Retallack 2009; Sosdian et al., 2018). From Figure 5A and Equation (2), we see that higher CO_2 correlates with higher A. However, this assumes that other variables are held constant. In reality, changes in CO_2 often affect other inputs in Equation (2), impacting the estimate of assimilation rate. For example, higher CO_2 usually selects for lower stomatal density and higher c_i/c_a
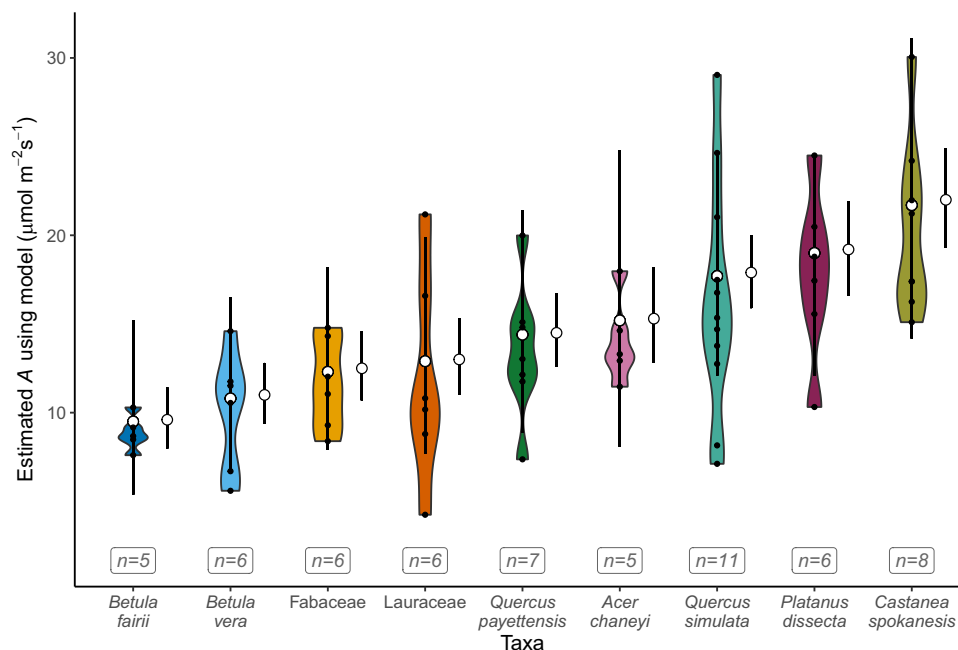
FIGURE 3   Violin plots showing species-level distributions of estimated assimilation rate (A) of nine fossil taxa from the Clarkia fossil lake. Hollow points represent median A. Filled points represent values of individual leaves ("n = "). Vertical lines in the violins represent 95% confidence in A at the species level assuming uncertainty propagation in all inputs; vertical lines to the right of the violins represent 95% confidence in A assuming no uncertainty in atmospheric CO_2.

(e.g., Franks et al., 2014), both of which would dampen the CO_2-driven increase in A (Figure 5B and D). Thus, what is shown in Figure 5A is the maximum effect.

Figure 6 shows a further sensitivity analysis for *Acer chaneyi*, which we consider a good representative taxon because its sensitivities in the first analysis (Figure 5) were close to the centerline relative to the other taxa. In this second analysis, we compare our standard run to an alternate run where all input uncertainties are set to zero except one. Once again, we find that plausible ranges in CO_2 have the most impact on estimated A (Figure 6). Indeed, the non-CO_2 inputs—including all the measured inputs and all the other inferred inputs like z—contribute less than 10% to the overall uncertainty in estimated A (compare "All" to "CO_2" in Figure 6).

Lastly, we ran our model including all uncertainties *except* atmospheric CO_2 concentration. These medians and 95% confidence bands are shown as the circles and vertical bars adjacent to the violins in Figure 3. These taxon-level uncertainties are much smaller than the standard runs, averaging +16%/−14% of the median estimates (vs. +51%/−38% for the standard runs), underscoring the model sensitivity to uncertainties in atmospheric CO_2. Indeed, the tighter mean confidence band is nearly identical to the modern test where the CO_2 uncertainty is essentially zero (+19%/−17%), suggesting that aside from the CO_2 uncertainty at Clarkia, the modern and fossil data sets have a similar level of precision. This restrictive case of assuming no uncertainty in atmospheric CO_2 is particularly relevant when comparing taxa within a fossil flora spanning minimal

stratigraphy, as CO_2 levels can be assumed to have been constant during the deposition of sampled leaf layers: that is, zero uncertainty in CO_2 across leaves, even if the absolute value of CO_2 is not known.

DISCUSSION

Model testing in living plants

We sought to create and test a model for rate of carbon assimilation in leaves (A) that can be readily applied to leaf fossils. We find that modelled A fits well with measured values for a group of ten extant species, including angiosperms, gymnosperms, and ferns (Figure 2). The validation of our model in living leaves shows promise in the accuracy of its estimates. The model precision (mean 95% confidence band of +19%/−17% of the median estimates at the species level) is generally better than tests on living plants of the vein density method (e.g., Sack et al., 2013); and unlike the NLR method, our method does not require an assumption of conserved physiology within a taxon over geologic time.

Application of model to fossil plants and implications for Clarkia forest

Significant overlap of reconstructed A occurs among the fossil taxa when uncertainty in CO_2 reconstructions is included (Figure 3). However, because the fossil plants were
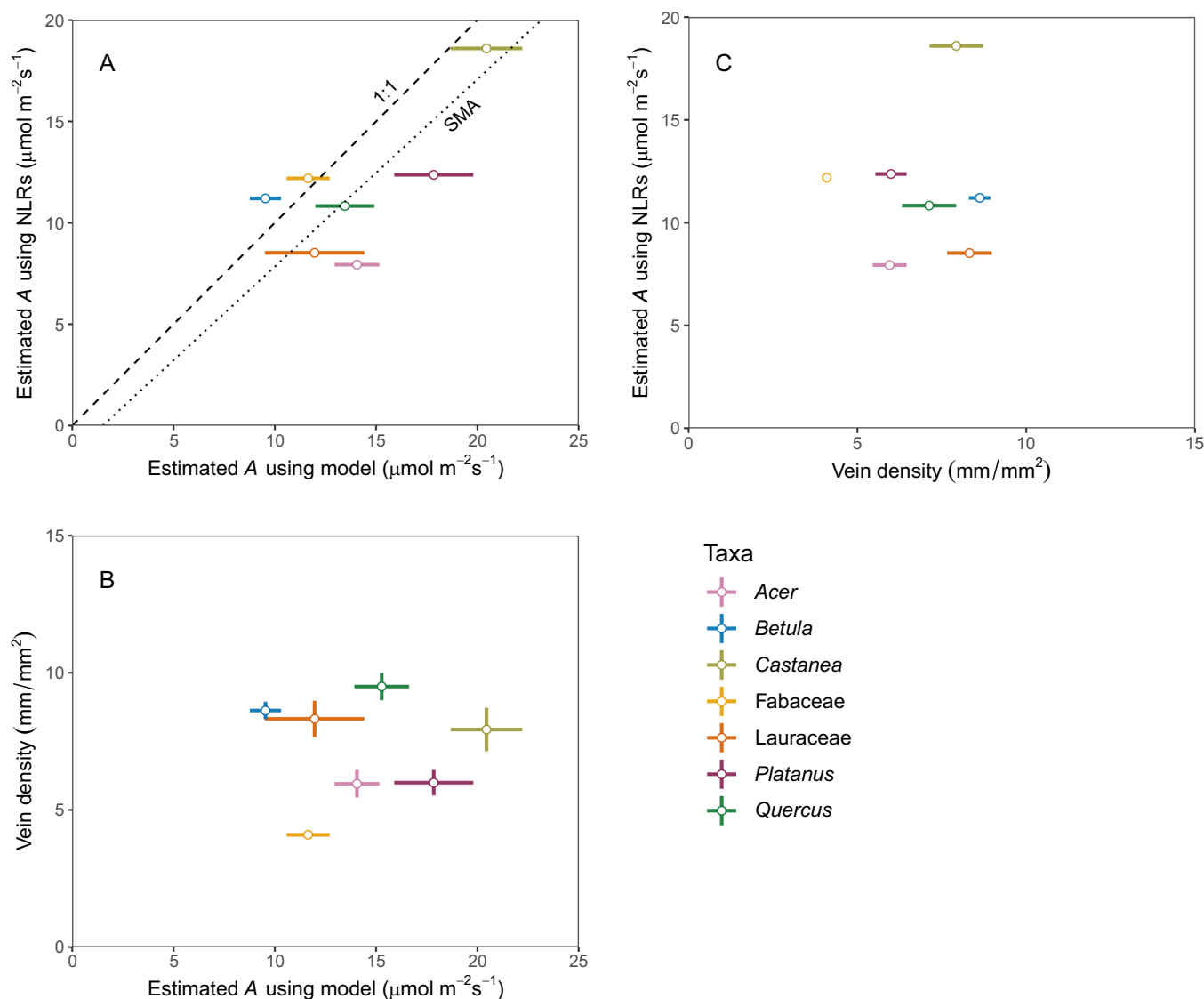
FIGURE 4 Comparison of three methods for constraining assimilation rates (A) at Clarkia. (A) Nearest living relative (NLR) versus our modeled A assuming a growth CO_2 concentration of 538 ppm. Dashed line shows 1:1 correlation. Dotted line shows standard major axis (SMA) regression: slope = 0.92, R^2 = 0.48, P = 0.09. (B) Fossil vein density versus our modeled A assuming Miocene CO_2 concentration of 538 ppm, showing no statistically significant correlation (P = 1.00). (C) NLR assimilation rate versus fossil vein density, showing no statistically significant correlation (P = 1.00). For all plots, error bars represent the standard error of the mean taken at the leaf level; for ease of comparison to the NLR data, *Betula* fossil data are consolidated at the genus level. *Quercus simulata* fossil data are not included in panels A and C because its generic affinity is unclear (Fields, 1996); nonetheless, the correlation patterns remain unchanged even when included (Appendix S7: Figure S1). Alternatively, assuming equivalence with modern *Lithocarpus* (Rember, 1991) does not make a difference (Appendix S7: Figure S2).

sampled from the same discrete 40 cm horizon, we can assume they existed in a similar CO_2 regime. Excluding CO_2 uncertainty from our model shrinks the confidence bands of reconstructed A and permits reliable characterizations of relative rank orders. Thus, our main interpretations focus on relative differences independent of our choice for atmospheric CO_2 concentration. Relative difference in reconstructed A reflects varying ecological strategies and can be used to test niche conservatism hypotheses: that is, relative ecological niches occupied by taxa are conserved across evolutionary time scales (DiMichele et al., 2004; Qian and Ricklefs, 2004; Tiffney, 2008).

Variation in rank orders of reconstructed A values of Clarkia taxa are in part consistent with previous interpretations of ecological strategies, ranging from plants with rapid growth and resource acquisition typical in high resource (e.g., disturbed) environments to 'slower' taxa typical of climax vegetation. For example, *Castanea spokanensis* and *Platanus dissecta* have comparatively high estimated A, which is in keeping with observation of fast growth in extant species of *Castanea* (Graves, 1905; McEwan et al., 2006; Wang et al., 2013) and *Platanus* (Burns and Honkala, 1990). *Quercus simulata* (="*Lithocarpus simulata*") an unlobed fagaceous species with uncertain generic affinity (see Rember 1991),
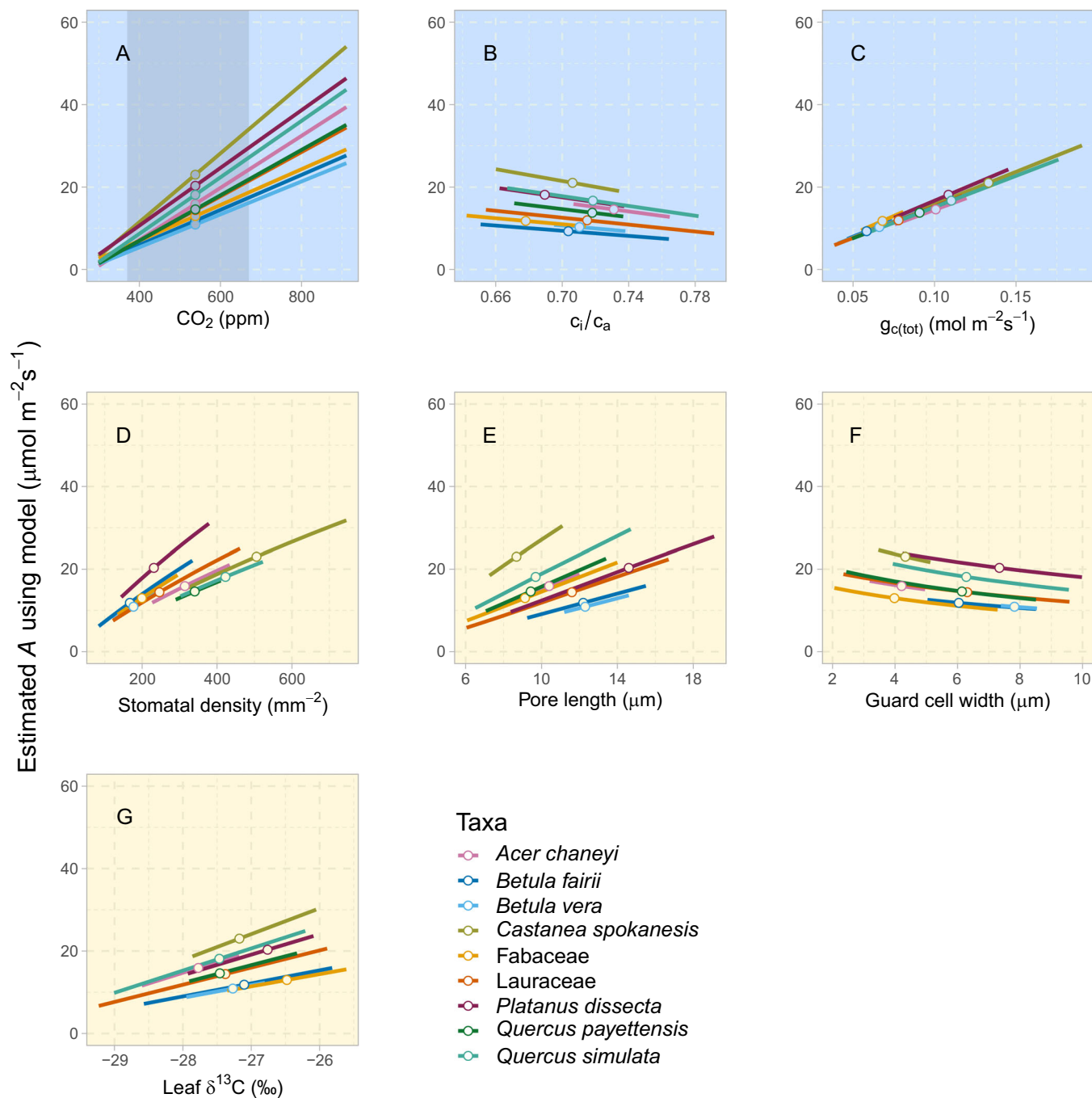
FIGURE 5   Sensitivity of assimilation rate (A) to some of the major inputs in the modified Franks model. The x-axis range for each taxon (colored line) captures the leaf-mean minimum to maximum, with the hollow circle representing the mean; for CO_2, the range comes from the compilation of Hönisch et al. (2023) (see Materials and Methods for details). Panels A–C are the three master variables of the model. Panels D–F are measured variables that contribute to $g_{c(tot)}$. Panel G is a measured variable that contributes to c_i/c_a. Shaded region in panel A is the 16th and 84th percentile of our CO_2 estimate based on Hönisch et al. (2023).

also has relatively high reconstructed *A*, agreeing with previous interpretations of its growth in well-lit (high resource) lacustrine environments (Axelrod, 1964); proximal and lakeside growth also agrees with its high abundance in the sampled Clarkia horizon (Appendix S7: Table S6). Together, these patterns provide support for niche conservatism over 15 million years.

The low *A* reconstructed for *Betula vera* and *B. fairii* (Figure 4A) are unexpected, as extant *Betula* species are typically fast-growing and shade intolerant (Burns and Honkala, 1990) and *Betula* leaves are abundant in the sampled Clarkia horizon (Appendix S7: Table S6). Alternatively, species of *Betula* at Clarkia may have in fact been slow-growing. The extant taxon *B. alleghaniensis*
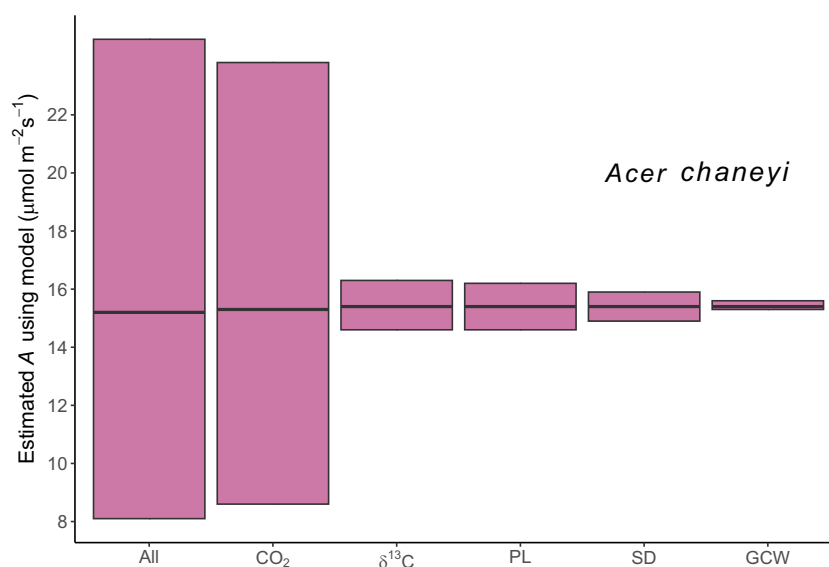
FIGURE 6 Contribution of uncertainty for inputs in our model for a representative species, *Acer chaneyi*, "All" is the standard run with all uncertainties included (identical to black vertical line inside violin in Figure 4). All other runs include only the uncertainty of the labeled input (CO_2 = atmospheric CO_2, $\delta^{13}C$ = leaf $\delta^{13}C$, PL = stomatal pore length, SD = stomatal density, GCW = single guard cell width). Lines and bars represent the median and 95% confidence band based on the "means" approach for aggregating leaf-level estimates of *A* into a taxon-level estimate (see *Model implementation*).

Britton—suggested as a close relative to *B. vera* (Chaney and Axelrod, 1959)—is fairly atypical among *Betula* in displaying intermediate shade tolerance and it can be abundant yet slow-growing in poorly drained wetland soils (Erdmann, 1990; Sullivan, 1994; Ward and Stephens, 1997). Thus, we suggest *Betula* species at Clarkia may have had a growth and ecological strategy similar to extant *B. alleghaniensis*, and that its slow growth was influenced by poorly drained soils in the surrounding ancient lakeside forest.

Overlap in an intermediate range of reconstructed *A* values across the remaining five taxa likely reflects similarities in their shade tolerance and growth environments or reflects intraspecific variability resulting from integration across diverse landscape patches of varying microenvironments (Ellsworth and Reich, 1993; Abrams, 1994; Šantrůček et al., 2014; Reichgelt and D'Andrea, 2019; Liu et al., 2023). Overlap could also be caused by incorporation of both shade and sun leaves that vary in *A* and stomatal traits (Ellsworth and Reich, 1993; Poole et al., 1996; Bassow and Bazzaz, 1997; Niinemets et al., 1998). Along with a higher *A*, sun leaves often have a higher vein density (Sack and Scoffoni, 2013) and higher d^{13}C (Lockheart et al., 1998) than shade leaves in the same species, but we generally do not find this pattern in our species (Appendix S7: Figure S3).

Recommendations for use

Although our method shows promise by reconstructing a plausible range of values for median *A* compared to modern trees and shrubs (Reichgelt and D'Andrea, 2019), a weakness is the large uncertainties associated with it, i.e., at Clarkia the average 95% confidence band for species is

+51%/−38% of the median estimates. By far the greatest contributor to this uncertainty is the uncertainty in atmospheric CO_2. Thus, future applications to fossil sites with well-constrained CO_2 may have tighter confidence bands that approach what we found both with our modern test and at Clarkia when excluding CO_2 uncertainty. We encourage future users to test the model's sensitivity to their suite of fossil data. For example, our values for c_i/c_a, stomatal size, and stomatal density at Clarkia capture only a narrow range of known values (Appendix S7: Figure S4). In other words, at sites where these inputs vary more widely within species, they may contribute more significantly to the overall uncertainty in estimated *A*.

Perhaps the most straightforward application of our method is for estimating relative *A* across or between fossil floras that can reasonably be assumed to have experienced invariant CO_2. As a fundamental aspect of the leaf-economic spectrum, estimates of paleo-assimilation rates can be used to reconstruct past growth strategies which cannot be directly measured in fossils. Reconstructing growth strategies is essential for understanding the ecology of ancient plant communities and the evolutionary ecology of plant lineages. For example, at Clarkia, several taxa are hypothesized to have had rapid growth and resource acquisition strategies (Wang et al., 2013), perhaps linked to volcanic disturbances during the mid-Miocene of the Pacific Northwest (Ladderud et al., 2015), whereas other taxa are thought to have had more slow-growing strategies (Sullivan, 1994). Our data support previous, NLR-based reconstructions of ecological strategy, providing evidence for niche conservatism among the taxa living near the Clarkia lake. Although we do not interpret absolute estimates of *A*, paleoecological strategies can still be inferred

from relative comparisons that complement other techniques such as NLRs. Our method adds to an expanding paleoecological toolkit allowing increasingly detailed understanding of past plant ecologies and ecosystem function.

AUTHOR CONTRIBUTIONS

ACKNOWLEDGMENTS

DATA AVAILABILITY STATEMENT

All data for this paper are available in the supplemental appendices.

ORCID

Melanie R. Cham https://orcid.org/0009-0006-2725-4539
Alexander J. Lowe https://orcid.org/0000-0002-2514-1008
Dana L. Royer https://orcid.org/0000-0003-0976-953X
Caroline A. E. Strömberg https://orcid.org/0000-0003-0612-0305

REFERENCES

Abrams, M. D. 1994. Genotypic and phenotypic variation as stress adaptations in temperate tree species: A review of several case studies. *Tree Physiology* 14: 833–842.

Ackerly, D. D., and P. B. Reich. 1999. Convergence and correlations among leaf size and function in seed plants: A comparative test using independent contrasts. *American Journal of Botany* 86: 1272–1281.

Axelrod, D. I. 1964. The Miocene Trapper Creek flora of southern Idaho. *University of California Publications in Geological Sciences* 51: 1–148.

Bassow, S., and F. Bazzaz. 1997. Intra-and inter-specific variation in canopy photosynthesis in a mixed deciduous forest. *Oecologia* 109: 507–515.

Blonder, B., C. Violle, L. P. Bentley, and B. J. Enquist. 2011. Venation networks and the origin of the leaf economics spectrum. *Ecology Letters* 14: 91–100.

Boyce, C. K., T. J. Brodribb, T. S. Feild, and M. A. Zwieniecki. 2009. Angiosperm leaf vein evolution was physiologically and environmentally transformative. *Proceedings of the Royal Society, B, Biological Sciences* 276: 1771–1776.

Brodribb, T. J., T. S. Feild, and L. Sack. 2010. Viewing leaf structure and evolution from a hydraulic perspective. *Functional Plant Biology* 37: 488–498.

Burns, R. M., and B. H. Honkala (eds.). 1990. Silvics of North America: Volume 2. Hardwoods. Agriculture Handbook 654. U.S. Department of Agriculture, Forest Service, Washington, District of Columbia, USA.

Chaney, R. W., and D. I. Axelrod. 1959. Miocene floras of the Columbia Plateau. Publication 617. Carnegie Institution of Washington, Washington, District of Columbia, USA.

Cornwell, W. K., J. H. C. Cornelissen, K. Amatangelo, E. Dorrepaal, V. T. Eviner, O. Godoy, S. E. Hobbie, et al. 2008. Plant species traits are the predominant control on litter decomposition rates within biomes worldwide. *Ecology Letters* 11: 1065–1071.

DiMichele, W. A., A. K. Behrensmeyer, T. Olszewski, C. C. Labandeira, J. M. Pandolfi, S. L. Wing, and R. Bobe. 2004. Long-term stasis in ecological assemblages: Evidence from the fossil record. *Annual Review of Ecology, Evolution, and Systematics* 35: 285–322.

Donovan, L. A., H. Maherali, C. M. Caruso, H. Huber, and H. de Kroon. 2011. The evolution of the worldwide leaf economics spectrum. *Trends in Ecology & Evolution* 26: 88–95.

Ellsworth, D., and P. Reich. 1993. Canopy structure and vertical patterns of photosynthesis and related leaf traits in a deciduous forest. *Oecologia* 96: 169–178.

Erdmann, G. 1990. *Betula alleghaniensis* Britton. *In* R. M. Burns and B. H. Honkala (eds.), Silvics of North America: Volume 2. Hardwoods. Agriculture Handbook 654, 133–147 U.S. Department of Agriculture, Forest Service, Washington, District of Columbia, USA.

Farquhar, G. D., and T. D. Sharkey. 1982. Stomatal conductance and photosynthesis. *Annual Review of Plant Physiology* 33: 317–345.

Fields, P. F. 1996. The Succor Creek flora of the Middle Miocene Sucker Creek Formation, southwestern Idaho and eastern Oregon: Systematics and paleoecology. Ph.D. dissertation, Michigan State University, East Lansing, Michigan, USA.

Franks, P. J., D. L. Royer, D. J. Beerling, P. K. Van De Water, D. J. Cantrill, M. M. Barbour, and J. A. Berry. 2014. New constraints on atmospheric CO_2 concentration for the Phanerozoic. *Geophysical Research Letters* 41: 4685–4694.

Geraghty, C. S. 2017. Tephrochronology of mid-Miocene Clarkia Lake Sedimentary Deposits. Masters thesis, Washington State University, Pullman, Washington, USA.

Graves, H. 1905. Notes on the rate of growth of red cedar, red oak and chestnut. *Journal of Forestry* 3: 349–353.

Greenop, R., G. L. Foster, P. A. Wilson, and C. H. Lear. 2014. Middle Miocene climate instability associated with high-amplitude CO_2 variability. *Paleoceanography* 29: 845–853.

Hobbs, K. M., and J. T. Parrish. 2016. Miocene global change recorded in Columbia River basalt–hosted paleosols. *Geological Society of America Bulletin* 128: 1543–1554.

Hönisch, B., D. L. Royer, D. O. Breecker, P. J. Polissar, G. J. Bowen, M. J. Henehan, Y. Cui, et al. 2023. Toward a Cenozoic history of atmospheric CO_2. *Science* 382: eadi5177.

Jones, T. P., and N. P. Rowe (eds.). 1999. Fossil plants and spores: Modern techniques. Geological Society of London, London, UK.

Kindt, R. 2020. WorldFlora: An R package for exact and fuzzy matching of plant names against the World Flora Online taonomic backbone data. *Applications in Plant Science* 8: e11388.

Kowalczyk, J. B., D. L. Royer, I. M. Miller, C. W. Anderson, D. J. Beerling, P. J. Franks, M. Grein, et al. 2018. Multiple proxy estimates of atmospheric CO_2 from an Early Paleocene rainforest. *Paleoceanography and Paleoclimatology* 33: 1427–1438.

Ladderud, J. A., J. A. Wolff, W. C. Rember, and M. E. Brueseke. 2015. Volcanic ash layers in the Miocene Lake Clarkia beds: Geochemistry, regional correlation, and age of the Clarkia flora. *Northwest Science* 89: 309–323.

Liang, J.-Q., Q. Leng, D. F. Höfig, G. Niu, L. Wang, D. L. Royer, K. Burke, et al. 2022. Constraining conifer physiological parameters in leaf gas-exchange models for ancient CO_2 reconstruction. *Global and Planetary Change* 209: 103737.

Liu, C., L. Sack, Y. Li, J. Zhang, K. Yu, Q. Zhang, N. He, and G. Yu. 2023. Relationships of stomatal morphology to the environment across plant communities. *Nature Communications* 14: 6629.

Lockheart, M., I. Poole, P. Van Bergen, and R. Evershed. 1998. Leaf carbon isotope compositions and stomatal characters: Important considerations for palaeoclimate reconstructions. *Organic Geochemistry* 29: 1003–1008.

Maxbauer, D. P., D. L. Royer, and B. A. LePage. 2014. High Arctic forests during the Middle Eocene supported by moderate levels of atmospheric CO_2. *Geology* 42: 1027–1030.

McElwain, J. C., W. J. Matthaeus, C. Barbosa, C. Chondrogiannis, K. O' Dea, B. Jackson, A. B. Knetge, et al. 2024. Functional traits of fossil plants. *New Phytologist* 242: 392–423.

McEwan, R. W., C. H. Keiffer, and B. C. McCarthy. 2006. Dendroecology of American chestnut in a disjunct stand of oak chestnut forest. *Canadian Journal of Forest Research* 36: 1–11.

Milligan, J. N., A. G. Flynn, J. B. Kowalczyk, R. S. Barclay, J. Geng, D. L. Royer, and D. J. Peppe. 2022. Moderate to elevated atmospheric CO_2 during the Early Paleocene recorded by *Platanites* leaves of the San Juan Basin, New Mexico. *Paleoceanography and Paleoclimatology* 37: e2021PA004408.

Milligan, J. N., D. L. Royer, P. J. Franks, G. R. Upchurch, and M. L. McKee. 2019. No evidence for a large atmospheric CO_2 spike across the Cretaceous-Paleogene boundary. *Geophysical Research Letters* 46: 3462–3472.

Murray, M., W. K. Soh, C. Yiotis, S. Batke, A. C. Parnell, R. A. Spicer, T. Lawson, et al. 2019. Convergence in maximum stomatal conductance of C_3 woody angiosperms in natural ecosystems across bioclimatic zones. *Frontiers in Plant Science* 10: 558.

Murray, M., W. K. Soh, C. Yiotis, R. A. Spicer, T. Lawson, and J. C. McElwain. 2020. Consistent relationship between field-measured stomatal conductance and theoretical maximum stomatal conductance in C_3 woody angiosperms in four major biomes. *International Journal of Plant Sciences* 181: 142–154.

Niinemets, Ü., O. Kull, and J. D. Tenhunen. 1998. An analysis of light effects on foliar morphology, physiology, and light interception in temperate deciduous woody species of contrasting shade tolerance. *Tree Physiology* 18: 681–696.

Poole, I., J. Weyers, T. Lawson, and J. Raven. 1996. Variations in stomatal density and index: Implications for palaeoclimatic reconstructions. *Plant, Cell & Environment* 19: 705–712.

Qian, H., and R. E. Ricklefs. 2004. Geographical distribution and ecological conservatism of disjunct genera of vascular plants in eastern Asia and eastern North America. *Journal of Ecology* 92: 253–265.

R Core Team. 2023. R: A language and environment for statistical computing. R Foundation for statistical computing, Vienna, Austria, version 2023.09.1+494. Website: https://www.R-project.org [accessed 23 June 2025].

Reich, P. B. 2014. The world-wide 'fast–slow' plant economics spectrum: A traits manifesto. *Journal of Ecology* 102: 275–301.

Reichgelt, T., and W. J. D'Andrea. 2019. Plant carbon assimilation rates in atmospheric CO_2 reconstructions. *New Phytologist* 223: 1844–1855.

Rember, W. C. 1991. Stratigraphy and paleobotany of Miocene lake sediments near Clarkia, Idaho. Ph.D. dissertation, University of Idaho, Moscow, Idaho, USA.

Retallack, G. J. 2009. Refining a pedogenic-carbonate CO_2 paleobarometer to quantify a middle Miocene greenhouse spike. *Palaeogeography, Palaeoclimatology, Palaeoecology* 281: 57–65.

Roeske, C., and M. H. O'Leary. 1984. Carbon isotope effects on enzyme-catalyzed carboxylation of ribulose bisphosphate. *Biochemistry* 23: 6275–6284.

Royer, D. L., and M. T. Hren. 2022. Bulk carbon isotopic variability within leaves. *Palaios* 37: 411–417.

Royer, D. L., K. M. Moynihan, M. L. McKee, L. Londoño, and P. J. Franks. 2019. Sensitivity of a leaf gas-exchange model for estimating paleoatmospheric CO_2 concentration. *Climate of the Past* 15: 795–809.

Sack, L., and C. Scoffoni. 2013. Leaf venation: Structure, function, development, evolution, ecology and applications in the past, present and future. *New Phytologist* 198: 983–1000.

Sack, L., C. Scoffoni, G. P. John, H. Poorter, C. M. Mason, R. Mendez-Alonzo, and L. A. Donovan. 2013. How do leaf veins influence the worldwide leaf economic spectrum? Review and synthesis. *Journal of Experimental Botany* 64: 4053–4080.

Šantrůček, J., M. Vráblová, M. Šimková, M. Hronková, J. Drtinová, J. Květoň, D. Vrábl, et al. 2014. Stomatal and pavement cell density linked to leaf internal CO_2 concentration. *Annals of Botany* 114: 191–202.

Schindelin, J., I. Arganda-Carreras, E. Frise, V. Kaynig, M. Longair, T. Pietzsch, S. Preibisch, et al. 2012. Fiji: An open-source platform for biological-image analysis. *Nature Methods* 9: 676–682.

Smiley, C. J., and W. C. Rember. 1985a. Physical setting of the Miocene Clarkia fossil beds, northern Idaho. *In* C. J. Smiley (ed.), Late Cenozoic history of the Pacific Northwest, 11–31. Pacific Division of the American Association for the Advancement of Science, San Francisco, California, USA.

Smiley, C. J., and W. C. Rember. 1985b. Composition of the Miocene Clarkia flora. *In* C. J. Smiley (ed.), Late Cenozoic history of the Pacific Northwest, 95–112. Pacific Division of the American Association for the Advancement of Science, San Francisco, California, USA.

Sosdian, S. M., R. Greenop, M. P. Hain, G. L. Foster, P. N. Pearson, and C. H. Lear. 2018. Constraining the evolution of Neogene ocean carbonate chemistry using the boron isotope pH proxy. *Earth and Planetary Science Letters* 498: 362–376.

Steinthorsdottir, M., H. K. Coxall, A. M. De Boer, M. Huber, N. Barbolini, C. D. Bradshaw, N. J. Burls, et al. 2021a. The Miocene: the future of the past. *Paleoceanography and Paleoclimatology* 36: e2020PA004037.

Steinthorsdottir, M., P. E. Jardine, and W. C. Rember. 2021b. Near-future pCO$_2$ during the hot Miocene Climatic Optimum. *Paleoceanography and Paleoclimatology* 36: e2020PA003900.

Sullivan, J. 1994. *Betula alleghaniensis*. *In* Fire Effects Information System [Online]. U.S. Department of Agriculture, Forest Service, Rocky Mountain Research Station, Fire Sciences Laboratory, Missoula, Montana, USA. Website: https://www.fs.usda.gov/database/feis/plants/tree/betall/all.html [accessed 29 October 2024].

Tiffney, B. H. 2008. Phylogeography, fossils, and Northern Hemisphere biogeography: The role of physiological uniformitarianism. *Annals of the Missouri Botanical Garden* 95: 135–143.

Tipple, B. J., S. R. Meyers, and M. Pagani. 2010. Carbon isotope ratio of Cenozoic CO_2: A comparative evaluation of available geochemical proxies. *Paleoceanography* 25: PA3202.

Wang, G. G., B. O. Knapp, S. L. Clark, and B. T. Mudder. 2013. The silvics of Castanea dentata (Marsh.) Borkh., American chestnut, Fagaceae (beech family). General Technical Report. SRS-GTR-173. U.S. Department of Agriculture, Forest Service, Southern Research Station, Ashville, North Carolina, USA.

Ward, J. S., and G. R. Stephens. 1997. Survival and growth of yellow birch (*Betula alleghaniensis*) in southern New England. *Canadian Journal of Forest Research* 27: 156–165.

Zhang, X., D. L. Royer, G. Shi, N. Ichinnorov, P. S. Herendeen, P. R. Crane, and F. Herrera. 2024. Estimates of late Early Cretaceous atmospheric CO_2 from Mongolia based on stomatal and isotopic analysis of *Pseudotorellia*. *American Journal of Botany* 111: e16376.

SUPPORTING INFORMATION

Additional supporting information can be found online in the Supporting Information section at the end of this article.

Appendix S1. R script for estimating assimilation rates.

Appendix S2.

Table S1. Estimating assimilation rates model input for fossil and living taxa.

Appendix S3. R script for scaling leaf-level probabilities to species-level probability.

Appendix S4.

Table S2. Example input file for scaling leaf-level probabilities to species-level probability.

Appendix S5. Supplemental methods for lifting leaves and $\delta^{13}C$ analysis.

Appendix S6.

Table S3. Guard cell width, pore length, guard cell length, stomatal denssity, and $\delta^{13}C$ fossil measurements.

Table S4. Vein density fossil measurements.

Table S5. Nearest living relative light-saturated photosynthetic carbon assimilation rate.

Appendix S7.

Figure S1. Comparison of three methods for constraining assimilation rates (*A*) at Clarkia. Similar to Figure 4 but includes *Quercus simulata*.

Figure S2. Comparison of assimilation rates between *Quercus simulata* and nearest living relatives of *Quercus* and *Lithocarpus*.

Table S6. Relative abundance and raw counts of the top 10 most abundant taxa samples from the studied horizon at Clarkia P37.

Figure S3. Comparisons of leaf $\delta^{13}C$, vein density, and estimated assimilation rates (*A*) for individual leaves within a taxon.

Figure S4. Comparison of c_i/c_a, stomatal density, and stomatal size at Clarkia P37 to published compilations.